Functional Group Identification in Scanning Tunneling Microscopy of Molecular Adsorbates

Donna M. Cyr,[†] Bhawani Venkataraman, and George W. Flynn*

Department of Chemistry and Columbia Radiation Laboratory, Columbia University, New York, New York 10027

Andrew Black and George M. Whitesides

Department of Chemistry, Harvard University, Cambridge, Massachusetts 02138

Received: February 29, 1996[⊗]

Monolayer films of several primary substituted hydrocarbons $CH_3(CH_2)_nCH_2X$ (X = CH_3, OH, NH_2, SH, Cl, Br, I; $n = 16-30$) have been imaged on graphite at the solution−substrate interface using a scanning tunneling microscope (STM). The straight chain hydrocarbons form well-ordered 2-D films on graphite and physisorb with their molecular axes parallel to the surface. The NH_2, SH, Br, and I end groups are observed as bright spots in the STM image corresponding to an enhancement in the tunnel current in the vicinity of the functional group, relative to the remainder of the carbon chain. On the other hand, the OH and Cl substituents were not distinguishable from the alkyl chain in the STM images. Comparison of the relative "brightness" of the functional groups with respect to the carbon chain reveals an empirical relationship between increasing relative brightness and increasing molecular polarizability. A model is proposed to describe the STM imaging mechanism for these insulating, physisorbed films in which the role of the adsorbate's polarizability, electronic structure, and orientation with respect to the surface are considered.

Introduction

The scanning tunneling microscope (STM) is capable of directly imaging with atomic resolution molecules at solution−solid interfaces and has recently been used to identify, possibly with chemical specificity, molecular adsorbates at interfaces.[1−3] Organic molecules, which are generally insulators, are typically studied by STM as thin films or as isolated molecules that permit electrons to flow between the STM tip and an underlying conductive substrate.[2,4−36] Aromatic[1,3,5−9] and sulfur[1,2] groups in physisorbed organic thin films display a much larger tunnel current than the remainder of the hydrocarbon molecule and appear as bright spots in the STM image. These "highlighted" functional groups are useful chemical markers that enable the molecular conformation or structure within a film to be interpreted even when atomic resolution is not achieved.[6−8,24,34] In the case of chemisorbed aromatics (e.g., anthracene and naphthalene) on Pt, the distinct internal structure of the adsorbates observed in the STM images[35] allows these structurally similar molecules to be identified and distinguished within a mixture. In this case, and others, the shapes of the adsorbates in the STM images are similar to the shapes of the HOMO (highest occupied molecular orbital) and LUMO (lowest unoccupied molecular orbital) of the molecules, suggesting that the frontier orbitals of these species participate in the tunneling process.[1,5,24,25,34,37,38] The STM tunneling probability is sensitive to the local density of states (LDOS) of the sample with energies close to the Fermi level and in close spatial proximity to the tip. It is not completely clear how the electronic states of insulating molecular adsorbates participate in the tunneling process since the HOMO and LUMO of these molecules lie several electronvolts away from the Fermi level of the tip and surface.[39,40] Despite the fact that the tunneling process for *molecular* adsorbates is not well understood, STM reveals detailed information on the molecular structure and dynamics within thin films.

Strong STM contrast has been observed for the atomic adsorbate Xe physisorbed on Ni(110). Lang and co-workers[41] proposed that the adsorbate image contrast is determined by the degree to which the adsorbate contributes to the LDOS at the Fermi level. This interpretation is of interest here because the large energy separation between Xe 5p and 6s (the highest occupied atomic orbital and the lowest unoccupied atomic orbital) places the isolated Xe orbitals several electronvolts away from the Ni Fermi level, an energy separation comparable to the typical HOMO−LUMO gap of an insulating organic molecule. Lang's model of the STM contrast for Xe on Ni provides a framework in which to interpret the STM image contrast of physisorbed molecular adsorbates. Other groups have proposed that molecular states may participate directly in the tunneling process and can be accessed as intermediates in the tunneling process.[18,25,32] From a different perspective, Spong and co-workers[4] propose that the corrugation or contrast of insulating molecules in STM images is due to modulation of the substrate's local work function (a modification of the barrier to tunneling) by the presence of the adsorbate. In this picture the STM simply maps out variations in the transmitted current through the perturbed barrier, thereby making the adsorbate "visible". Polarizability is one important factor in determining the adsorbate's effect on the surface work function and hence the adsorbate contrast.[42−44] Both benzene and cyclohexane, for example, have similar polarizabilities and exhibit similar strong ("bright") contrast in the STM even though their electronic structures are quite different.[4]

"Highlighted" functional groups in STM images of physisorbed hydrocarbon films, such as aromatic and sulfur groups, are unlikely to be unique. In this paper we survey the relative "brightness" of several functional groups (−CH_3, −OH, −Cl, −NH_2, −SH, −Br, −I) attached to long chain hydrocarbons

[†] Marie Curie Postdoctoral Fellow sponsored by the American Association of University Women.

[⊗] Abstract published in *Advance ACS Abstracts,* June 1, 1996.

S0022-3654(96)00646-6 CCC: $12.00

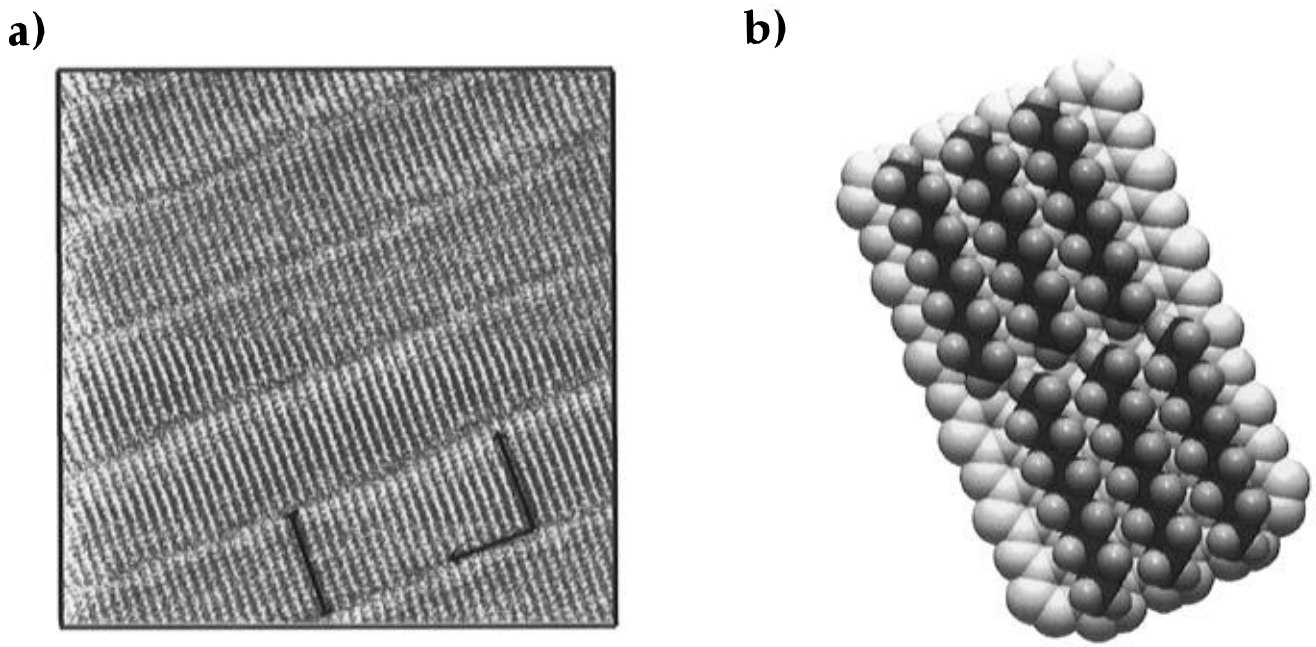

Figure 1. (a) STM image of triacontane ($C_{30}H_{62}$) in phenyloctane physisorbed on graphite. One molecular length is represented by a black bar. The molecules are oriented with a 90° angle between the molecular axis and the direction of the lamellae. The 20 nm^2 image was obtained with a 1235 mV bias (sample negative) and a 166 pA set point in constant height mode. (b) Computer-generated model of an all-trans alkane film on a graphite substrate.

physisorbed on graphite in order to identify other bright functional groups. Additionally, we attempt to correlate variations in the functional group brightness with physical properties of the adsorbates. The empirical trends in the image contrast are discussed in the context of the proposed imaging mechanisms involving the role of the sample's LDOS and polarizability, respectively. Additionally, the discovery of "highlighted" functional groups in STM images may identify potentially useful markers for interpreting structure in STM images of more complex molecular systems.

Experimental Section

A Digital Instruments Nanoscope III scanning tunneling microscope was employed to investigate functionalized hydrocarbon films physisorbed on graphite at the solution/solid interface. 1-Chlorooctadecane ($CH_3(CH_2)_{17}Cl$), 1-bromodocosane ($CH_3(CH_2)_{21}Br$), 1-iodooctadecane ($CH_3(CH_2)_{17}I$), 1-triacontanol ($CH_3(CH_2)_{29}OH$), triacontane ($CH_3(CH_2)_{28}CH_3$), and 1-octadecylamine ($CH_3(CH_2)_{17}NH_2$) were obtained from Aldrich and used without further purification. The 1-docosanethiol ($CH_3(CH_2)_{21}SH$) was synthesized as described elsewhere.[45] Nearly saturated solutions of these compounds were made in a phenyloctane solvent with the exception of chlorooctadecane (a liquid at room temperature), which was applied directly to the graphite surface. The phenyloctane was purged with N_2 to remove any residual oxygen dissolved in the solvent prior to preparing the solutions. A drop (~10 μL) of solution was deposited on a freshly cleaved piece of highly ordered pyrolytic graphite (HOPG, from Advanced Ceramics Corp.). All the images were collected under ambient conditions at temperatures between 19 and 23 °C. The STM tips were mechanically clipped from a 0.01 in. Pt/Rh (87/13) wire (Omega) using diagonal cutters. Once the sample was mounted, the STM tip was immersed into the liquid droplet and the images were obtained under the solution. The typical range of tunneling conditions used for this group of samples was 1200−1600 mV (sample negative) and 80−400 pA with the STM operating in either the constant current or constant height modes. Under these conditions the tip−surface separation is much larger than when imaging the bare graphite surface (~50 mV and 1 nA). In some cases the images were subjected to a single low pass filter. Each of the images presented here is representative of several images taken at different times to ensure reproducibility.

Space-filling molecular models (shown in the figures with 85% van der Waals radii) were constructed using Macromodel,[46] a molecular mechanics software package. Models of the hydrocarbon films were created with the molecules in an orientation consistent with the STM images. The molecular film was then docked onto a graphite "slab", simulating the HOPG surface, and subsequently subjected to energy minimization using an AMBER force field.[47] The resulting adsorbate/substrate model structures have many degrees of freedom and may not correspond to the lowest energy configurations; however, they provide a representation of the adsorbate films consistent with the STM images.

Results

Alkanes and Alcohols. Long chain alkanes and alcohols were some of the first hydrocarbons to be imaged at the solution/solid interface since they form well-ordered films on graphite near room temperature.[10−12,23,30] The images of these molecules are presented again here for comparison to the STM images of films with other functional end groups. An STM image of a triacontane ($C_{30}H_{62}$) film physisorbed on graphite is shown in Figure 1a. One molecular length is indicated by a black bar in the image. The molecules appear to be fully extended, indicating an all-trans conformation along the hydrocarbon backbone. Straight chain alkanes on graphite are generally characterized by a 90° angle between the molecular axis and the direction of the rows or lamellae, as shown in the model in Figure 1b. This packing orientation maximizes the interactions between the hydrocarbon chains, thereby stabilizing the film. Additionally, the graphite substrate acts as a template for formation of the hydrocarbon film in which the hydrogens of the alkyl chains are believed to reside in the hollow sites of the graphite lattice. The good lattice match between the alkyl

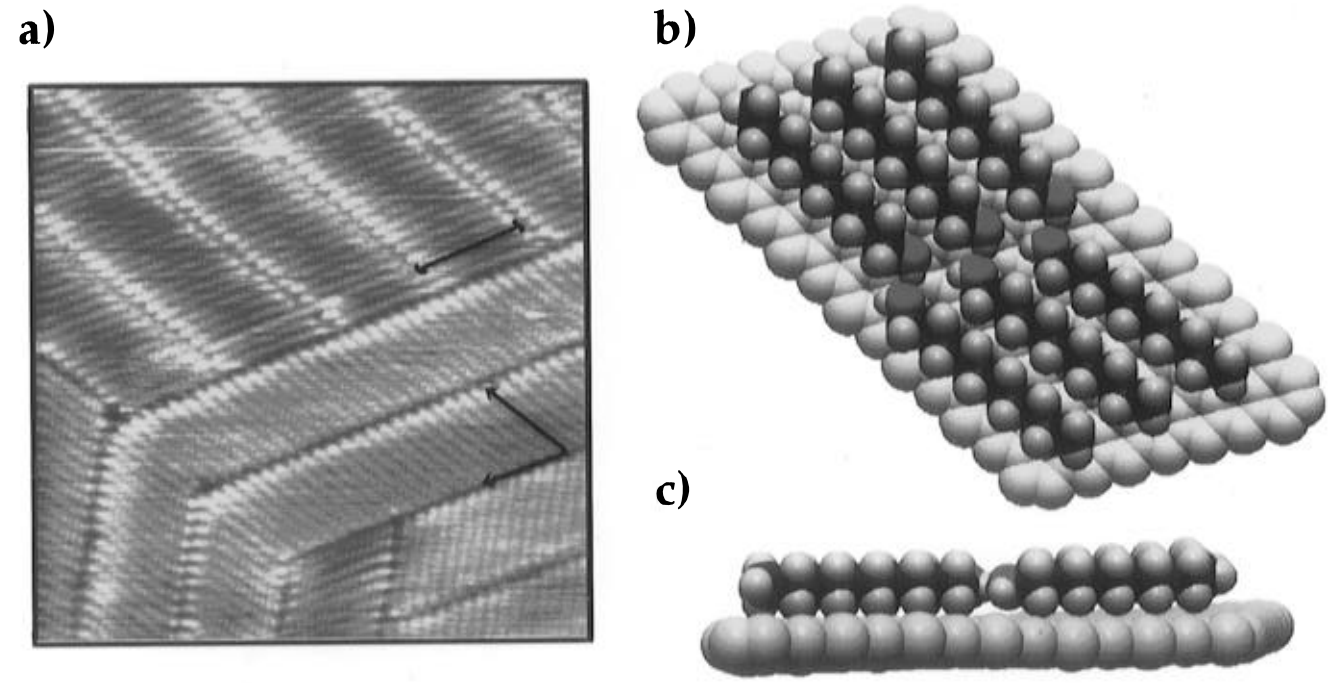

Figure 2. (a) STM image of triacontanol ($CH_3(CH_2)_{29}OH$) in phenyloctane on graphite. One molecular length is indicated by a black bar. The molecules are oriented with a 60° angle between the molecular axis and the direction of the lamellae, as indicated on the image. The 20 nm^2 image was obtained with a 1400 mV bias (sample negative) and an 80.0 pA set point in constant current mode. (b) Top view of a computer-generated model of an alcohol film on graphite. The hydrogen bonding of the alcohols within the film requires the OH groups of the molecules in adjacent rows to lie "head to head". (c) Side view of the model shown in b showing that the OH groups lie in the plane of the film.

backbone and the graphite lattice favors commensurate packing of the hydrocarbon film with the underlying substrate.[10,48−50]

Two domains are observed in the image of triacontanol ($C_{30}H_{61}OH$) on graphite which appear to follow the lattice directions of the underyling graphite surface. The $C_{30}H_{61}OH$ film on graphite is characterized by a 60° angle between the molecular axis and the direction of the lamellae (Figure 2a). The relative orientation of the alcohol molecules is defined by the hydrogen-bonding network in the film, in contrast to the 90° angle observed for the alkanes in which no hydrogen bonding can occur. Hydrogen bonding requires that the OH groups of molecules in adjacent rows lie "head to head" in the film, as shown in Figure 2b. Similar STM contrast is observed over the entire molecule in most of our images of alcohol films, although in some instances one or both ends of the molecules appear brighter than the central portion of the alkyl chain. From our images it is not apparent that the STM is "sensitive enough" to distinguish the OH end group from the remainder of the hydrocarbon backbone in the images of these molecules. Similar contrast features have been reported by Elbel et al. for the alcohols on graphite.[51] In mixtures, the alcohols and the alkanes tend to segregate into separate domains on the surface and have been differentiated in mixtures by their respective, functionally specific packing orientations. These individual systems have been described in more detail elsewhere.[10]

Sulfur. Functional group specificity has recently been observed for several sulfur-containing hydrocarbons: 1-docosanethiol ($CH_3(CH_2)_{21}SH$),[2] docosane disulfide ($CH_3(CH_2)_{21}SS(CH_2)_{21}CH_3$),[2,52] octadecyl sulfide $CH_3(CH_2)_{17}S(CH_2)_{17}CH_3$),[52] and dihexadecyl disulfide ($CH_3(CH_2)_{15}SS(CH_2)_{15}CH_3$).[1] In the STM images of these molecules an enhancement in the tunnel current is observed in the vicinity of the sulfur group. An STM image of 1-docosanethiol ($CH_3(CH_2)_{21}SH$) on graphite is shown in Figure 3a. The bright spots in the image of the thiol correspond to an increase in the tunnel current in the vicinity of the SH end group, while the C_{22} alkyl chain is observed as a thin band of darker contrast. In this image the molecules appear to be lying flat with their molecular axis parallel to the graphite surface. The thiol molecules lie preferentially "head to head" (the SH groups facing each other), while a few lie "head to tail" (SH group to CH_3 terminated end), as shown in the computer model of a thiol film on graphite in Figure 3b. The thiols appear to pack with a 90° angle between the molecular axis and the direction of the row, similar to the alkane films (see Figure 1a), indicating that the SH···S interaction in the thiol film is much weaker than the OH···O hydrogen bond in the alcohol film. The enhanced tunneling associated with the thiols has also been reported for aromatic groups in thin molecular films, although sulfur is one of the first "atomic" functionalities observed with this property in a physisorbed organic film. Elemental specificity has been observed recently for STM images of clean semiconductor alloy surfaces (InGaAs and GaAsP).[53]

Amines. In an attempt to search for other functional groups which may be distinguishable with the STM, we examined films of octadecylamine ($CH_3(CH_2)_{17}NH_2$) on graphite, as shown in Figure 4a. Like many other hydrocarbons on graphite, the amine molecules orient parallel to each other in well-ordered rows, creating a 2-D crystalline film. The length of one molecule (indicated by a black bar) agrees well with the expected length for a fully extended, all-trans conformation and indicates that the molecules lie flat with their molecular axis parallel to the graphite surface. The angle between the molecular axis of the amines and the direction of the lamellae is about 60°. This is reminiscent of the molecular orientation observed for the alcohol films presented in Figure 2a. The amines in nonpolar solvents such as phenyloctane, like the alcohols, form a hydrogen-bonding network which defines the molecular orientation within the monolayer.

Unlike the alcohols, one end of the $CH_3(CH_2)_{17}NH_2$ molecule is observed to have a "brighter" contrast than the rest of the C_{18} alkyl chain. Presumably, the bright ends of the molecules mark the location of the NH_2 groups. NH_2 groups appear to be paired in a "head to head" orientation, thereby creating a

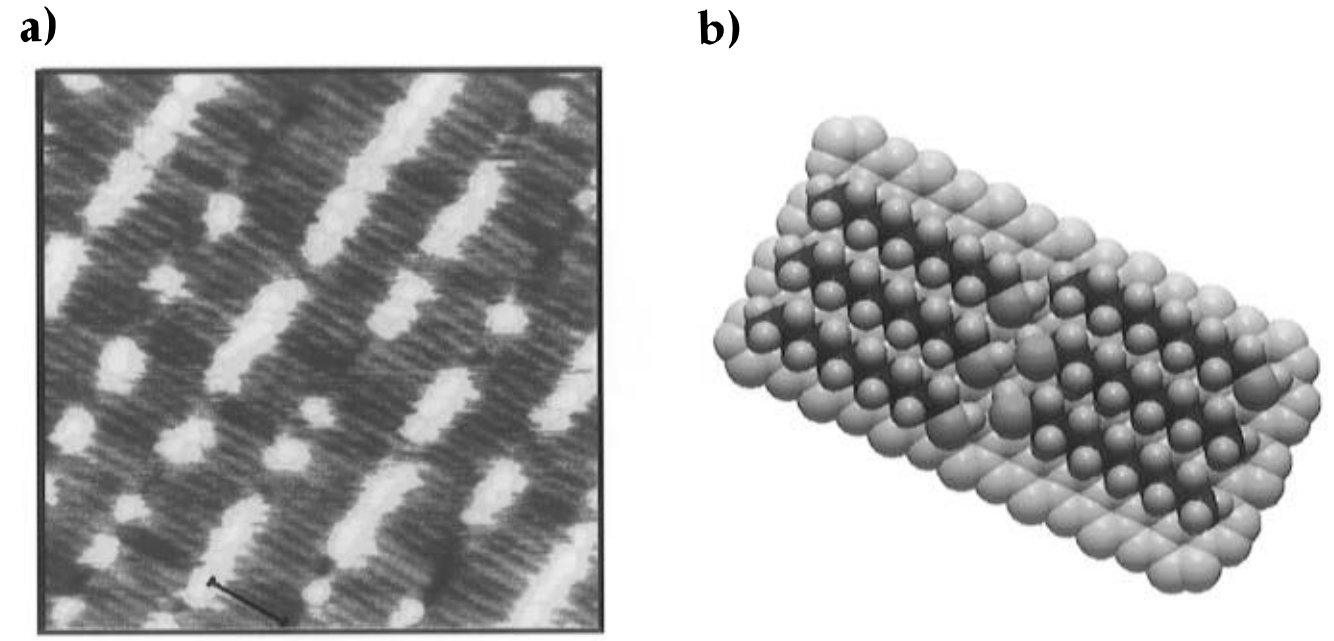

Figure 3. (a) STM image of 1-docosanethiol ($CH_3(CH_2)_{21}SH$) in phenyloctane on graphite. One molecular length is indicated by a black bar. The image is dominated by bright spots which indicate the positions of the SH groups. The 20 nm^2 image was obtained with a 1550 mV bias (sample negative) and a 150.0 pA set point in constant current mode. (b) Top view of a computer-generated model of a thiol film on a graphite substrate. The SH groups are preferentially oriented "head to head" but occasionally orient "head to tail".

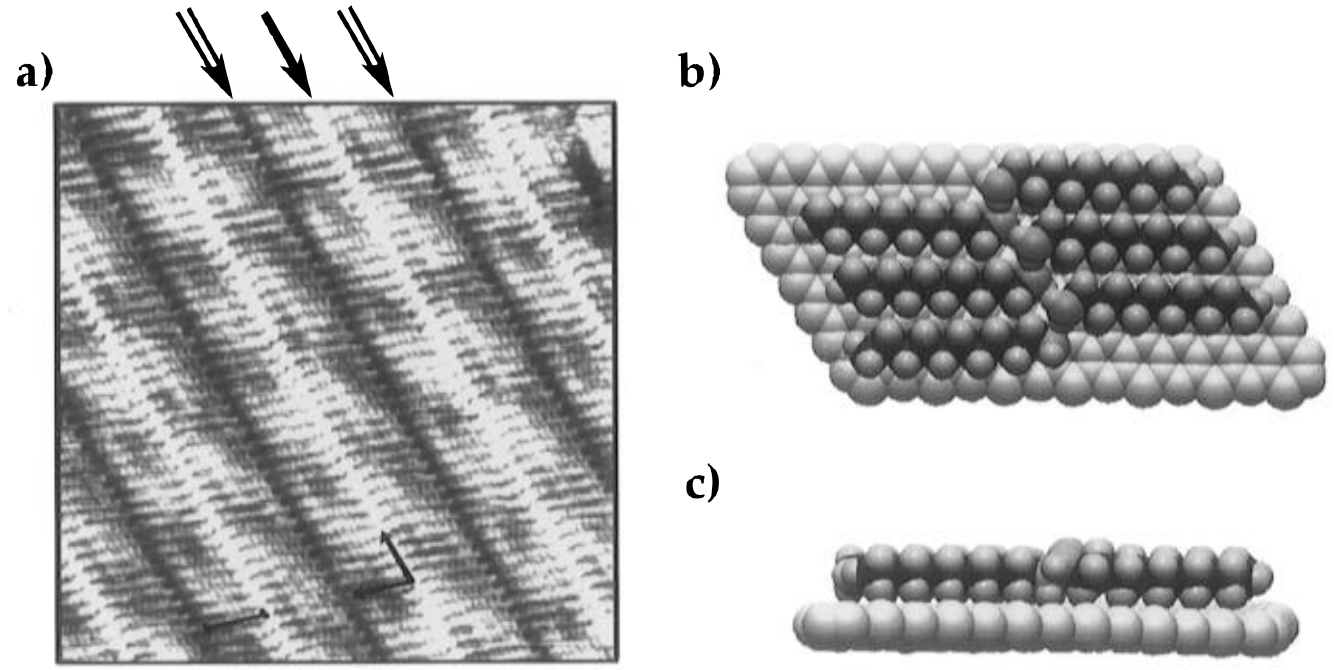

Figure 4. (a) An STM image of 1-octadecylamine ($CH_3(CH_2)_{17}NH_2$) in phenyloctane on graphite. One molecular length is indicated by a black bar. The angle between the molecular axis and the direction of the lamellae is 60°. The rows of molecules appear to be paired with the position of the NH_2 groups observed as a bright line (indicated by →). The rows of molecules are separated by deep troughs (indicated by ⇒). The 20 nm^2 image was obtained with a 1500 mV bias (sample negative) and a 150.0 pA set point in constant current mode. (b) Top view of computer-generated model of an amine film on a graphite substrate. Hydrogen bonding between the amine groups in the film defines the molecular orientation. (c) Side view of the model in b, showing that the lone pair of the amine N atom points out of the film in this structure. This is in contrast to the orientation of OH groups, which lie in the plane of the alcohol film shown in Figure 2c.

bright "center line" joining the molecules in the paired rows (marked by → in Figure 4a). The other end of the molecule has the same contrast as the rest of the alkyl chain and is separated from the adjacent row by a deep trough (marked by ⇒). A "head to head" orientation is also necessary for hydrogen bonding between molecules within the film, and a model consistent with these observations is presented in Figure 4b.

The image of the amines (Figure 4a) also displays an intensity variation in the "background" contrast from dark to bright, or a moiré pattern, which appears with a repeat over about four to five molecules. This type of contrast variation has been observed in other films such as carboxylic acids on graphite[12] and has been attributed to a molecular film which is incommensurate with the underlying graphite lattice. Incommensurate packing of the film may occur if the intermolecular interactions (van der Waals and electrostatic forces) between functionalized hydrocarbons within the film are stronger than the molecule−surface interactions which lead to commensurate packing. The

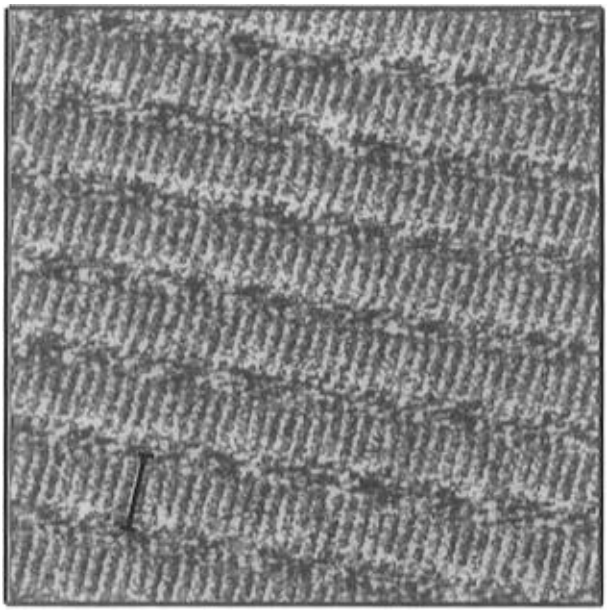

Figure 5. STM image of 1-chlorooctadecane ($CH_3(CH_2)_{17}Cl$) in phenyloctane on graphite. One molecular length is indicated by a black bar. The 20 nm^2 image was obtained with a 1500 mV bias (sample negative) and a 120 pA setpoint in constant height mode.

contrast variation appears to be most pronounced when there is a mismatch between the substrate surface and the films along both unit vectors of the substrate lattice and indicates that the STM is sensitive to contributions from both the substrate and the molecular overlayer. In fact the moiré pattern has recently been used to determine the relative orientation of the adsorbate molecules with respect to the surface with high resolution.[54]

Halogens. Halogen-containing hydrocarbons are a convenient set of molecules in which to survey trends in the image contrast since the trends in physical properties of these molecules are well-defined. We have previously investigated octadecyl chloride ($CH_3(CH_2)_{17}Cl$) on graphite,[2] as shown in Figure 5. The molecular axis of the chlorides appears to form a 90° angle with the direction of the rows or lamellae, and these molecules have an image similar in appearance to that of the alkanes (Figure 1a). In this case the location of the chlorine atom could not be discerned from the STM images since similar contrast is observed on both ends of the molecule.

An STM image of 1-bromodocosane $CH_3(CH_2)_{21}Br$ film on graphite is shown in Figure 6a. A black bar indicates one molecular length. A 90° angle between the molecular axis and the lamellae direction is observed in the bromide film, similar to the arrangement observed in the alkane film (Figure 1a). Both ends of the molecule display similar contrast, and the terminal bromine is not directly distinguishable in this image. The troughs between the rows of molecules are observed with different contrast as marked by the arrows (→ and ⇒, the "narrow" and "wide" troughs, respectively) in Figure 6a and indicate an asymmetry between the two ends of the molecule. The asymmetric row spacings suggest that the rows of bromide molecules may be paired in a "head to head" orientation, as indicated in Figure 6b. It is unclear from this image alone in which trough the terminal bromides reside.

When the same region of the film is monitored continuously over a period of time (>10 min), a reversible change in the STM contrast is observed. As shown in Figure 7a, one end of the $CH_3(CH_2)_{21}Br$ molecule becomes "highlighted" by an increase in tunnel current. The bright spots appear to indicate the position of the bromine end group, confirming the specula-

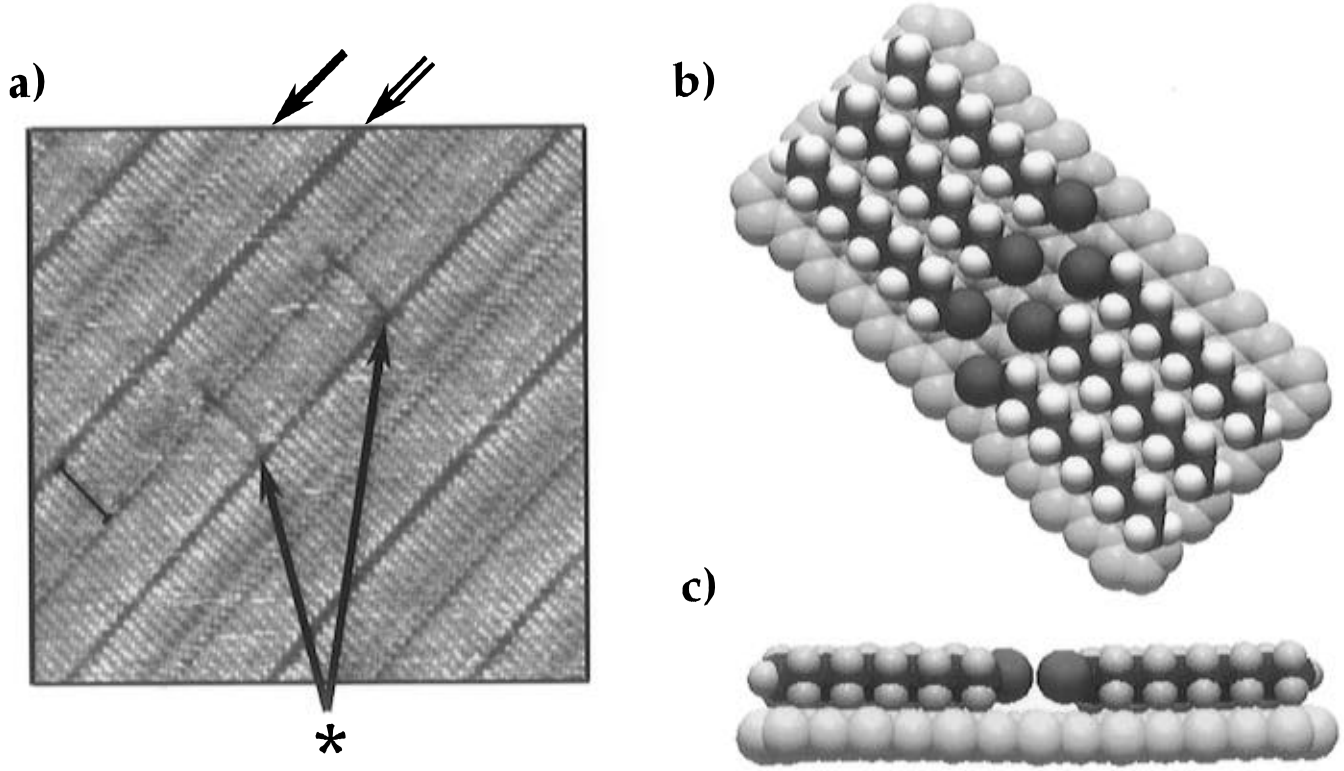

Figure 6. (a) An STM image of 1-Bromodocosane ($CH_3(CH_2)_{21}Br$) in phenyloctane on graphite. One molecular length is marked by a black bar. The troughs separating the rows of molecules indicated by → and ⇒, respectively, are not equivalent. The film has two defects, as marked by an asterisk, and are also apparent in Figure 7a. The 20 nm^2 image was obtained with a 1500 mV bias (sample negative) and a 400.0 pA set point in constant current mode. (b) Top view of a computer-generated model of a bromide film on a graphite substrate. In this model of the bromide film the rows of molecules are paired with the bromides oriented "head to head". (c) Side view of the model in b showing that the bromine end groups lie in the plane of the film for an all-trans conformation of the molecule.

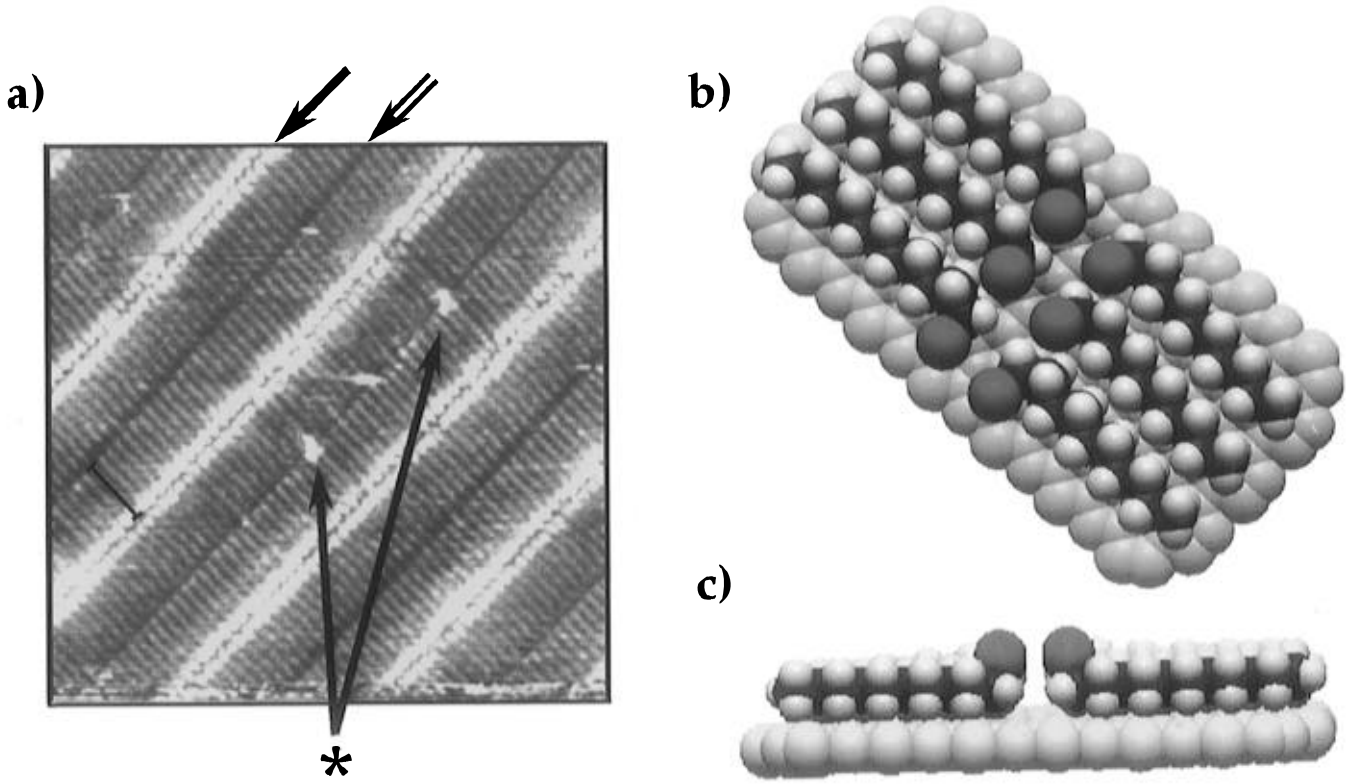

Figure 7. (a) STM image of 1-bromodocosane ($CH_3(CH_2)_{21}Br$) in phenyloctane on graphite taken approximately 10 min after the image in Figure 6a. No changes were made in the scan parameters between these images. The location of the bromines in the film are now indicated by bright spots at the ends of the molecule (→) and verify that the bromines lie "head to head". The film has two defects, marked by an asterisk, which are attributed to molecules with orientations opposite to the rest of the molecules in the film. These defects are also apparent in Figure 6a. The 20 nm^2 image was obtained with a 1500 mV bias (sample negative) and a 400.0 pA set point in constant current mode. (b) Top view of a computer-generated model of a bromide film on a graphite substrate. The bromide molecules shown in this model are in an end-gauche conformation in contrast to the all-trans conformation shown in Figure 6b. The bromide molecules in this model were oriented in an end-gauche geometry *prior* to energy minimization in order to locate the local minima around this conformation. Rotation about the terminal RCH_2-CH_2Br bond from a trans to a gauche conformation may be responsible for the changes observed in the image contrast. (c) Side view of the model in b showing that the bromine points up out of the film when in the end-gauche conformation.

tion that the bromides lie "head to head". This reversible contrast variation fluctuates spontaneously from "dark" to "bright" (with no changes in the microscope conditions) over a time scale of several minutes. The transition between bright and dark contrast occurs quickly (much faster than the time scale required to collect a single frame) and over a wide region, sometimes greater than 50 $Å^2$. These solution/solid interfaces are quite fluxional in general; however, once a large ordered domain is established, the molecular monolayer appears to remain stable for many minutes, allowing several images of the same area to be collected. The nature of the contrast variation will be considered below.

We have also investigated films of 1-iodooctadecane ($CH_3(CH_2)_{17}I$) on graphite shown in Figure 8. The image is dominated by lines of bright contrast which transect the STM images and presumably mark the location of the iodine end group. The spacing between the bright rows corresponds to two molecular lengths, indicating that the iodides lie "head to head" in the overlayer similar to the orientation of the bromides in Figure 6b. Unlike the bromides, the iodides always appear with a "bright" contrast, and no change in the contrast was observed with time. Individual iodide molecules ($CH_3(CH_2)_{17}I$) are observed with lower resolution than the bromides ($CH_3(CH_2)_{21}Br$, Figures 6 and 7). The shorter chain iodides are associated with a smaller heat of adsorption[48−50] (18 versus 20 carbons), which may result in a higher mobility of the iodides on the surface. Additionally, the large size of the iodine end group may also reduce the stability of the chain/chain interactions in the close packed film and allow greater motion within the film, thereby lowering the resolution. The presence of the large iodine substituent may also be a factor contributing to the appearance of a moiré pattern across the chains, suggesting that the molecular packing is incommensurate with the underlying graphite lattice.

Relative Intensities of the Functional Groups. As described above, large variations in the STM image contrast between hydrocarbons with several different end groups ($-CH_3$, $-OH$, $-NH_2$, $-SH$, $-Cl$, $-Br$, $-I$) have been observed under similar tunneling conditions. To make reliable comparisons among the contrasts for each of the functional groups, we attempted to correct for variations in the tunneling conditions from sample to sample by using the contrast of the alkyl chain in each sample as a reference. An integration box, approximately the size of the functional end group, was used to determine the average intensity over the functional group, the alkyl chain, and the background between the rows of chains. From these measurements, the "brightness" of each functional group, I_x, averaged over the area associated with the end group, was normalized to an average brightness associated with the remainder of the alkyl chain, I_a. The relative "brightness" of each of the functional groups, I_x*, was subsequently calculated according to eq 1:

$$I_x^* = (I_x - I_b)/(I_a - I_b) \quad (1)$$

where a background correction was made by subtracting the average intensity in a region between molecules, I_b, from the uncorrected intensities I_x and I_a. In the case where the end

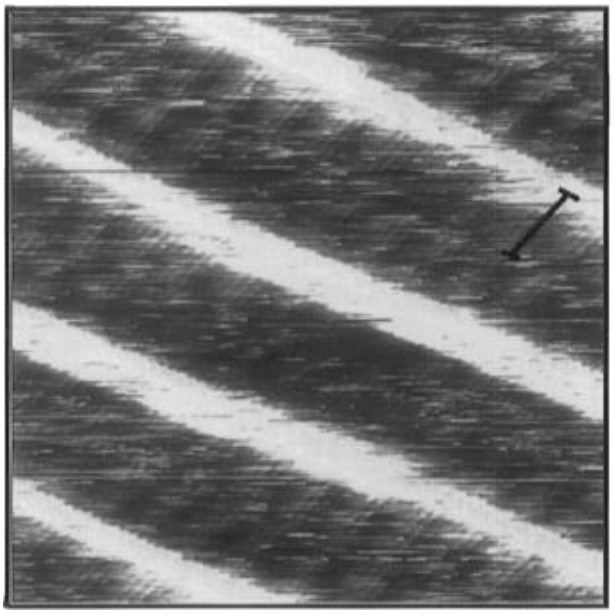

Figure 8. STM image of 1-iodooctadecane ($CH_3(CH_2)_{17}I$) in phenyloctane on graphite. One molecular length is indicated by a black bar. The image is dominated by bright lines which appear to indicate the location of the iodine atoms in the film. The separation between these "bright" lines is consistent with two molecular lengths and indicates that the iodides lie head to head. The 20 nm^2 image was obtained with a 1500 mV bias (sample negative) and a 250.0 pA set point in constant current mode.

TABLE 1: STM Functional Group Brightness Relative to the Brightness of the Alkyl Chain

functional group	relative brightness
CH_3	1.0[a]
OH	1.0[a]
Cl	1.0[a]
NH_2	1.3
Br	2.0[b]
I	3.0
SH	3.1

[a] Terminal functional group is not distinguishable from the remainder of the alkyl chain. [b] Only "bright" bromine images (similar to Figure 7a) were used in this calculation.

groups were not distinguishable from the remainder of the alkyl chain ($-CH_3$, $-OH$, and $-Cl$), it was assumed that $I_x = I_a$, and each of these groups was assigned a relative brightness (I_x*) of 1. Measurements from several different images were averaged, and the results are summarized in Table 1.

Discussion

General Trends in the Image Contrast. The STM has demonstrated sensitivity to several functional groups, including $-S$, $-NH_2$, $-Br$, and $-I$ (in addition to aromatic groups), while $-OH$ and $-Cl$ were not distinguishable from the hydrocarbon backbone for the molecules investigated here. The relative "brightness" of the substituents is observed to increase over the series $-CH_3 \sim -OH \sim -Cl < -NH_2 < -Br < -I < -SH$, as summarized in Table 1. Comparison of the relative contrast of the Cl, CH_3, OH, and SH end groups in an earlier study[2] led to the conclusion that the total electron density and electronegativity of a functional group are not the key factors in determining the magnitude of the observed tunneling current. The atomic electron affinity (EA) might be a possible factor governing the tunneling process since the substituent with the largest EA (Cl > Br > I) could be expected to interact most strongly with the tunneling electrons and thereby display the largest STM image contrast. The relative "brightness" of the halogens (R−Cl < R−Br < R−I, R = alkyl chain) in the STM image however displays the opposite trend, suggesting that the atomic EA of the substituent is not an important factor governing the tunneling contrast.

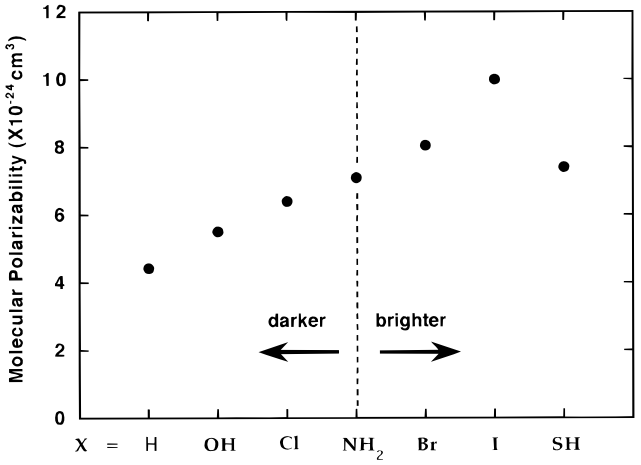

Figure 9. Plot of the molecular polarizability of C_2H_5X for each of the functional groups (X = H, OH, Cl, NH_2, SH, Br, I) examined in this study. Comparison of the observed "brightness" of the functional groups in Table 1 with the trends in the polarizability shows a correlation between increasing brightness and increasing polarizability. The designations of the functional groups as "dark" and "bright" describes the observed "brightness" of the functional group relative to the remainder of the alkyl chain as defined by eq 1.

It is well-known that the surface work function changes in the presence of polarizable adsorbates, and the measured tunnel current should increase as the barrier is reduced.[42,43] This implies that there may be a correlation between the adsorbates' polarizabilities and the STM image contrast when comparing different functional groups. To examine any correlation between the polarizability and the STM image contrast, the molecular polarizabilities of the ethyl-substituted hydrocarbons (C_2H_5X)[55] are plotted in Figure 9 in order of increasing STM image brightness for each of the functional groups studied here (X = H, OH, Cl, NH_2, SH, Br, I). The polarizabilities of the substituted ethanes were chosen for this comparison since the molecular polarizabilities of the long chain hydrocarbons investigated here have not been measured. The plot displays a correlation between increasing STM image brightness and increasing molecular polarizability over the set of functional groups examined.

Comparison of the relative contrast of the functional groups in Table 1 and the trends in the polarizabilities in Figure 9 shows that the groups with brighter contrast in the STM images (I_x* > 1 for X = NH_2, Br, I, and SH) have larger polarizabilities than their darker counterparts (I_x* = 1 for X = CH_3, OH, and Cl). While aromatic substituents were not investigated in this study, it should be noted that the polarizability of benzene is quite similar to that of ethyl iodide, and both benzene substituents in molecular films on graphite and the iodide film studied here are characterized by bright spots in the STM image. Our results are also in good agreement with the observation of Stevens et al.[3] in which both bromine and benzyl groups, within the same molecule, appear as bright spots in the STM image (the aromatic being noticeably brighter than the bromine). The notable exception to the trend in the polarizability is the $-SH$ end group, which suggests that additional factors may also contribute to the STM image contrast.

It is generally accepted that the STM tunneling probability reflects the local density of states (LDOS) at the Fermi level of

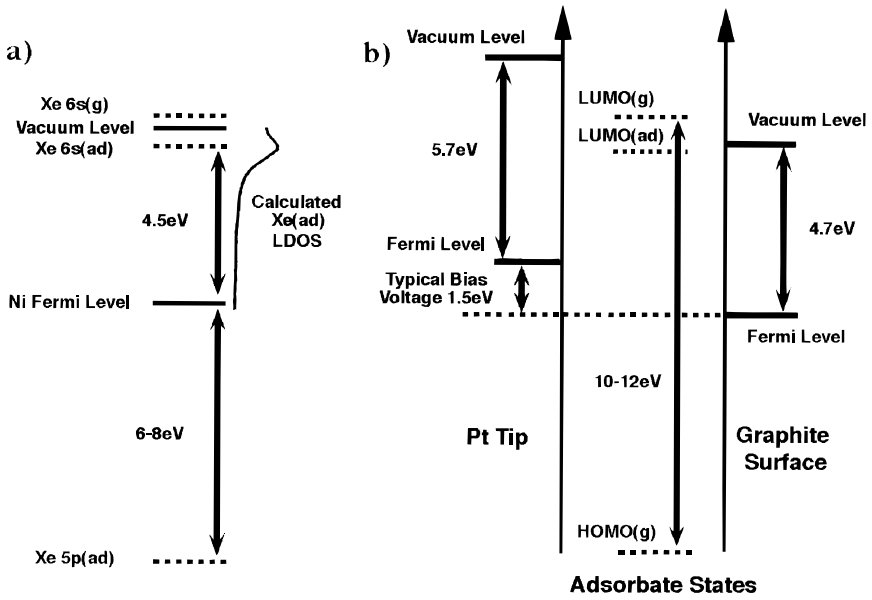

Figure 10. (a) Energy level diagram for Xe adsorbed on a Ni surface. Both the highest occupied Xe 5p and lowest unoccupied Xe 6s levels lie far in energy from the Ni Fermi level. Prior to adsorption, the gas phase Xe 6s(g) level lies just above the vacuum level. Upon adsorption the Xe 6s(ad) is lowered ~0.5 eV below the vacuum level by the heat of adsorption. Lang's atom on jellium calculation of the contribution of the Xe(ad) to the local density of states of the surface/adsorbate complex reveals that the resonance corresponding to the Xe 6s(ad) state is broadened upon adsorption and develops a long energy tail which extends to the Ni Fermi level (ref 41). Although the contribution of the Xe to the surface LDOS at the Fermi level is small (typically 1%), it is a weak function of the energy separation between the Fermi level and the Xe 6s state and, most importantly, pushes the spatial distribution of the electronic wave function far away from the surface (ref 41). (b) General qualitative energy level diagram for a molecular adsorbate on graphite with a typical HOMO−LUMO gap of 10−12 eV. Organic molecules are normally insulators, and the location of the HOMO and LUMO in the tunnel junction is not well-defined. However, by analogy with the Xe on Ni states in a, the adsorbate levels most likely lie far in energy (several electronvolts) from the Fermi levels of the graphite substrate and the Pt tip.

the surface being imaged.[56,57] Lang and co-workers[41] have considered the role of adsorbate energetics and electronic structure on the STM image contrast for the model case of atomic Xe adsorbed on Ni using an atom on jellium model. Similar to the physisorbed hydrocarbons, the isolated Xe atoms display strong contrast in the STM despite the large gap (~12 eV) between the highest occupied (5p) and lowest unoccupied (6s) atomic orbitals, which lie far in energy from the Fermi level of Ni. However, when the Xe atom adsorbs onto the surface, the gas phase 6s(g) level is lowered in energy by the heat of adsorption (see Figure 10a). The resulting adsorbed Xe 6s(ad) state lies ~0.5 eV below the vacuum level. While the Xe 6s(ad) retains a mostly Xe 6s(g) character, symmetry breaking upon physisorption allows weak mixing of the unoccupied 6s(g) with other Xe atomic states (of different symmetries) and some Ni surfaces states. The contribution of the Xe 6s(ad) to the LDOS was calculated by subtracting the bare Ni LDOS from the Xe plus Ni LDOS, at a large distance from the surface probed by the STM tip (~11 bohr).[41] This calculation revealed that the contribution of the Xe adsorbate to the LDOS (or the mixed surface/Xe 6s(ad) levels) is peaked 0.5 eV below the vacuum level. The normally sharp atomic 6s resonance for isolated Xe is broadened by the interaction between the surface and the adsorbed atom, exhibiting a width of roughly 0.5 eV. The key feature of these calculations, however, is that far away (>1.5 eV) from this Xe 6s resonance the contribution of the Xe states to the local density of states of the system becomes a very weak function of the energy, falling off only very slowly (see Figure 10a). Thus, although the contribution of Xe to the local density of states at energies well below that of the isolated lowest unoccupied 6s atomic orbital is small, it does not change very much with energy. Since the tunneling probability depends on the local density of states at the Fermi level, the imaging of adsorbates should not depend sensitively on the electronic structure of the adsorbate as long as the energy difference between the lowest unoccupied adsorbate level and the surface Fermi level is large. In addition this picture also predicts that the tunneling current should be strongly affected if the lowest unoccupied level of the adsorbate approaches within ~0.5 eV of the surface Fermi level (since the resonance's fwhm is ~0.5 eV).

The two cases, lowest unoccupied adsorbate level far from and near to the surface Fermi level, are somewhat analogous to ordinary and resonant Raman scattering. In ordinary Raman scattering the nonresonant interaction of a primary light beam with the tails of high-energy electronic states makes the scattering probability insensitive to the difference between the photon energy and the energy of electronic levels in the scattering medium. On the other hand a considerable enhancement in Raman scattering probability is observed when the photon energy approaches the energy separation of the ground and electronically excited levels in the medium. Similar to nonresonant Raman scattering, the energetically diffuse "tail" of the Xe 6s(ad) interacts with the Ni Fermi level, far in energy from the peak of the Xe resonance, to produce a small probability of tunneling.

Another key feature of these calculations for the theoretically tractable Xe on Ni system is that, despite the weak mixing of the Xe 6s and surface Fermi level electronic wave functions, the contribution of the adsorbate to the local density of states at the Fermi level is ~2 orders of magnitude larger than the contribution of the bare substrate to the LDOS at the large distances from the surface typically probed by the STM tip in an experiment where adsorbates are being imaged.[41] This is not surprising, of course, since the adsorbate sits on top of the surface, which *a priori* guarantees that its electronic wave function will be localized much farther out from the surface than can be expected for the electronic levels of the bare surface. These observations suggest that Xe becomes visible in the STM because the Xe adsorbate spatially dominates the region probed by the STM tip, despite the Xe 6s(ad) level's weak mixing with the Fermi level surface wave function. The STM can thereby

image the Xe through spatial overlap between the adsorbate and the tip and the residual state density of the Xe6s(ad) tail at the Fermi level.[41]

In the case of Xe on Ni the energies of the Xe adsorbate electronic levels are known from experiment, while for the functionalized organic adsorbates studied here the location of the LUMO level of the adsorbate with respect to the surface Fermi level energy is unknown. Nevertheless, Xe physisorbed on Ni, with a 5p−6s gap of ∼12 eV, appears to be the atomic analog of the insulating molecular adsorbates studied here since organic molecules typically have large HOMO−LUMO gaps of 8-12 eV. Recent experiments by Harrison et al. on CH_3Br/Xe/CH_3Br overlayers on Pt(111) place the LUMO of the topmost layer of CH_3Br in resonance with the Xe 6s approximately 0.5 eV below the vacuum level.[40] While the exact placement of the long chain hydrocarbon adsorbate levels with respect to the surface Fermi level is uncertain in the present studies, the frontier orbitals of the molecular adsorbates, like the Xe 6s on Ni, almost certainly lie several electronvolts away the Fermi level of the graphite surface or the Pt tip, as schematically shown in Figure 10b. By analogy to Xe on Ni, the frontier orbitals of insulating organic molecules should participate in the tunneling process through a weak mixing of the adsorbate LUMO and the electronic levels of the graphite at the Fermi level. The spatial extension of the molecule away from the surface pushes the mixed adsorbate/surface electronic wave function out from the surface where the contribution of the bare graphite to the Fermi level LDOS is negligible. This may explain how the tunneling electrons can couple to the molecular framework of these insulating molecules and why the shapes observed with the STM sometimes resemble the shape of the frontier orbitals.

This picture provides a number of insights that can be used to interpret much of the data observed in the present set of experiments involving a series of different adsorbates. To a first approximation, we assume that the electronic structure of the adsorbate is not critical since the adsorbate LUMO energy is likely to be far from the Fermi level of the bare graphite. In such cases (nonresonant interactions between the surface electronic states and the adsorbate electronic states) any feature of the adsorbate that pushes the spatial extent of its electronic wave function farther above the surface will enhance the tunnel current associated with the adsorbate or specific functional groups on the adsorbate. The most obvious of these factors is simply the size of the adsorbate or a specific functional group of the material, which is measured well by the polarizability of the adsorbate (the highly polarizable Xe, for example, is quite large, pushing its electronic wave function far from the surface of Ni). A second factor, one unavailable to spherically symmetric atomic Xe on Ni, is the geometric isomerization that can occur for molecular adsorbates. In the present series of molecules, this corresponds to whether functional groups bury themselves in the surface (point down), are parallel to the surface, or protrude from the surface. The third factor, which can affect the spatial extent of the adsorbate or functional group is the shape or localization of the LUMO. To the extent that this level and energetically nearby levels of the adsorbate are localized on a given functional group or stick up significantly from the surface, the tunneling into these spatially localized states will be enhanced at distances far from the bare surface.

Finally, of course, the electronic energy level structure of the adsorbate and the strength of its coupling to the surface (the degree of mixing of the surface electronic levels and the adsorbate electronic states) will come into play. In cases where the adsorbate's LUMO levels come near to the surface Fermi level, one expects a large enhancement in the mixing of these states and a concomitant enhancement in the tunneling probability (analogous to the situation that occurs with resonant Raman scattering). It should also be noted that, unlike atomic adsorbates, molecular adsorbates often have many electronically excited states that are close in energy to each other. When many such levels begin to mix with the Fermi level of the surface, especially if these levels are far in energy from the Fermi level (nonresonant case), the mixing should become less sensitive to the energy difference between the electronically excited level of the adsorbate and the Fermi level of the surface. (Again the analogy to nonresonant Raman scattering is appropriate here since the Raman effect is due to the interaction of a light beam of low photon energy with the "tails" of many high-energy electronically excited states.) In principle any of the frontier orbitals can make some contribution to the contrast observed in the STM images, but for simplicity we have neglected the participation of the adsorbate HOMO in our discussion of the tunneling process.

By analogy with the case of Xe on Ni, the LUMO might be expected to dominate the STM image contrast of these physisorbed films if the adsorbate LUMO lies closer in energy to the surface Fermi level than the distant HOMO, as depicted in Figure 10a. In such cases the smaller energy difference between the LUMO and the Fermi level could be expected to provide a stronger coupling and thereby, a relatively large contribution of the LUMO to the STM contrast. Nevertheless, as noted above, the energy gap between the Fermi and HOMO/LUMO levels is expected to be large, resulting in a weak dependence of the coupling on the energy gap. For adsorbates with small HOMO−LUMO gaps (i.e. aromatics), both the adsorbate HOMO and the LUMO can be expected to have a significant contribution to the STM image contrast.[34,37,38,58,59]

The present study establishes a good correspondence between adsorbate polarizability and image contrast. The possibility that the adsorbate directly participates in the tunneling process by contributing to the LDOS through an energetically broadened adsorbate LUMO, as discussed above, is appealing and appears to be consistent with much of the data obtained in the present study. We have also obtained some preliminary data indicating that Br and S substituents maintain bright STM image contrast (relative to the alkyl chain) over a wide range of bias voltages, from ±(2.0 to 0.5) eV.[60] The large changes in bias voltage are accompanied by loss of resolution along the alkyl chain, and for bias voltages smaller than ±0.5 eV, features of the graphite substrate begin to dominate the image.[57] Similar voltage dependences have been reported in the STM images of fatty acids on graphite by Hibino et al.[61] While these results are not definitive, they are consistent with the involvement of an energetically diffuse adsorbate LUMO participating in the tunneling process. The contribution of a broadened adsorbate LUMO to the sample density of states should not depend strongly on energy, (i.e. no resonances in the LDOS near the Fermi level energy),[41] suggesting that the contrast in the STM images of polarizable adsorbates should be relatively insensitive to bias voltage. Additionally, these results appear to rule out the likelihood of resonant tunneling through spatially localized and energetically "narrow" states, as has been observed in the differentiation of metals through their image potential states,[62] where sharp changes in the image contrast with bias voltage are observed.

The simple correlation between STM image contrast and adsorbate polarizability may arise from the weak dependence of the sample's LDOS (for the species studied here) on bias voltage, making the size of the functional group a primary factor

in determining the image contrast. However, the correlation of the polarizabilities with STM contrast is not perfect. From the trend of increasing polarizability, $-CH_3 < -OH < -Cl < -NH_2 < -SH < -Br < -I$ (see Figure 9), one might expect Br and I to be "brighter" than SH. However, SH is the brightest functional group observed here (Table 1). This disparity may be related to the details of the electronic structure of the sample and/or the tip. As mentioned earlier, when the energy difference between the adsorbate LUMO and the Fermi level is narrowed, the shoulder of the broadened LUMO may begin to contribute more strongly to the LDOS at the Fermi level and result in an enhancement in the tunnel current (the onset of resonant tunneling). In such cases, larger electronic mixing of the surface and adsorbate wave functions augments the contribution due to the effective spatial overlap between the tip and the adsorbate at large distances from the surface. The gas phase molecular EA locates the relative position of a molecule's LUMO with respect to the vacuum level. Unfortunately the thiol EA, to our knowledge, has not been measured, and a comparison of the relative proximity of each of the sample's LUMOs to the substrate's Fermi level (or vacuum level) cannot yet be made.

Contrast Variation in $CH_3(CH_2)_{21}Br$ Films. The $CH_3(CH_2)_{21}Br$ films display a contrast variation over time (Figures 6 and 7), and we consider here the factors which may control the changes in the image contrast. Since these images are collected at the solution−solid interface, the contrast variation may simply be due to the mobility of molecules into and out of the film, resulting in different molecules, possibly with different orientation or surface geometry, being imaged at different times. However, exchange of molecules between the solution and the adsorbate film is usually associated with some disordering or loss of resolution from molecular motion during the course of the experiment; this is *not* observed. Piezo drift with time may also be potentially responsible for the film contrast variations since drift would lead to imaging different regions of the film from frame to frame. Two defects in the bright bromide film (indicated by an asterisk in Figure 7a) can be employed as reference points and are identifiable as among the few molecules that are oriented with their "bright" bromine terminated end in the trough rather than aligned with the other "bright" spots within the row (marked by →). These defects appear to have corresponding analogs in the darker bromide film (indicated by an asterisk in Figure 6a). Additionally, the relative positions of the troughs (indicated by → and ⇒) in both images (Figures 6a and 7a) run throughout the same portion of the frame. These observations affirm the stability of the piezo with time and rule out the possibility that the contrast variation is simply due to the imaging of different areas of the film.

In an attempt to correlate the positions of the bromines in the dark and bright films, we compared the average cross-sectional profiles of both the dark and bright films (see parts b and d of Figure 11, respectively). Examination of an average cross-sectional profile of the bromide image perpendicular to the direction of the rows (and parallel to the molecular axis) reveals alternating "deep" and "shallow" troughs, as shown in Figure 11b. In this cross-sectional profile of the "dark" image the bromine is not distinguishable from the remainder of the alkyl chain and appears to lie in the plane of the film. Comparison of the profiles for the dark and bright images reveals a good correspondence between the location of the shallow trough (→, Figure 11a,b) in the dark image and the appearance of bright spots in the bright image (⇒, Figure 11c,d). The deep troughs (⇒), indicating the separation between rows of molecules on the methyl terminated end, remain deep in both profiles (Figure 11b,d) with approximately the same depth (∼0.025 nm). The absolute height scale in these images is not calibrated, but is consistent between the images considered here. It can be considered that the bromine resides in the shallow troughs of the darker image and exhibits "higher" contrast relative to the alkyl chain in the bright image, suggesting that the bromine may be sticking up out of the film.

Since the long chain adsorbates are quite flexible and are mobile at the solution/solid interface, the observed changes in the STM image contrast may reflect variations in the conformation (or orientation) of the molecules in the film. In general these physisorbed films are formed a few degrees below the melting point of the bulk hydrocarbon. As the melting point is approached, such crystals have been observed to undergo rotational phase transitions which mark the onset of disorder in the transition from the solid to the liquid phase.[63−69] These rotator phases near the melting point of the crystal are characterized by disorder due to pseudofree rotation of the alkanes about their molecular axis, which begins by rotation at the chain ends.[63−66] Reports of such disorder in bulk crystals from diffraction data are correlated with an increase in the chain−chain spacing in the crystal.[68] However no discernible change in chain−chain spacing is observed for the bromide film in Figures 6a and 7a as the contrast changes from dark to bright. Changes in the density of the film would not be observed if molecular reorganization occurs only at the ends of the molecules, corresponding to a trans−gauche isomerization around the terminal C−C bond, as shown with the models in Figures 6b,c and 7b,c respectively. The energy difference between the gauche and trans conformers of 1-bromopropane is quite small, ∼0.1 kcal/mol[70,71] (less than $RT \approx 0.6$ kcal/mol), with a slight preference for the gauche conformer. Interconversion between the two rotatomers should be feasible at the experimental temperatures in this study if the barrier to rotation is small. Trans−gauche isomerization may provide a mechanism for the ends of the molecules to reorient in the film, resulting in a change in the STM image through variation in the effective spatial "overlap" between the tip and adsorbate in the tunnel junction, as noted in the model above based on the Xe/Ni interaction. Note that in the "dark" STM image of the bromides (Figure 6a) we speculate that the bromines lie in the plane of the film with molecules in an all-trans conformation (Figure 6b), which results in poor overlap between the bromine and the tip. On the other hand, if the molecule undergoes rotational isomerization to the gauche form (Figure 7b), the spatial extent of the bromine's electronic wave function will protrude farther above the surface, enhancing the tunnel current associated with the bromine end group, and result in the bright spots observed in the STM image (Figure 7a). As discussed above, such a geometric rearrangement has the effect of pushing the adsorbate LUMO wave function farther out from the surface, thereby enhancing the tunnel current associated with the specific Br functional group on the adsorbate. Rotation of the entire molecule around its long axis, proposed for the bulk alkane rotator phases, may also be another plausible rearrangement mechanism.[63−66]

The close proximity of the molecules within the film may orchestrate these motions in a concerted fashion, explaining why the change in contrast is observed to occur rapidly over a large domain. In fact, a "meshed gear" model[65] has been proposed for the motion of rotator phases in bulk crystals, since the barrier to rotation in the condensed phase would be relatively high without cooperation between neighboring molecules. Evidence of cooperative reorganization within physisorbed organic films has been reported experimentally[5,7,15,18,72] and in molecular dynamics[73] simulations. In films of 2-hexadecylanthraquinone

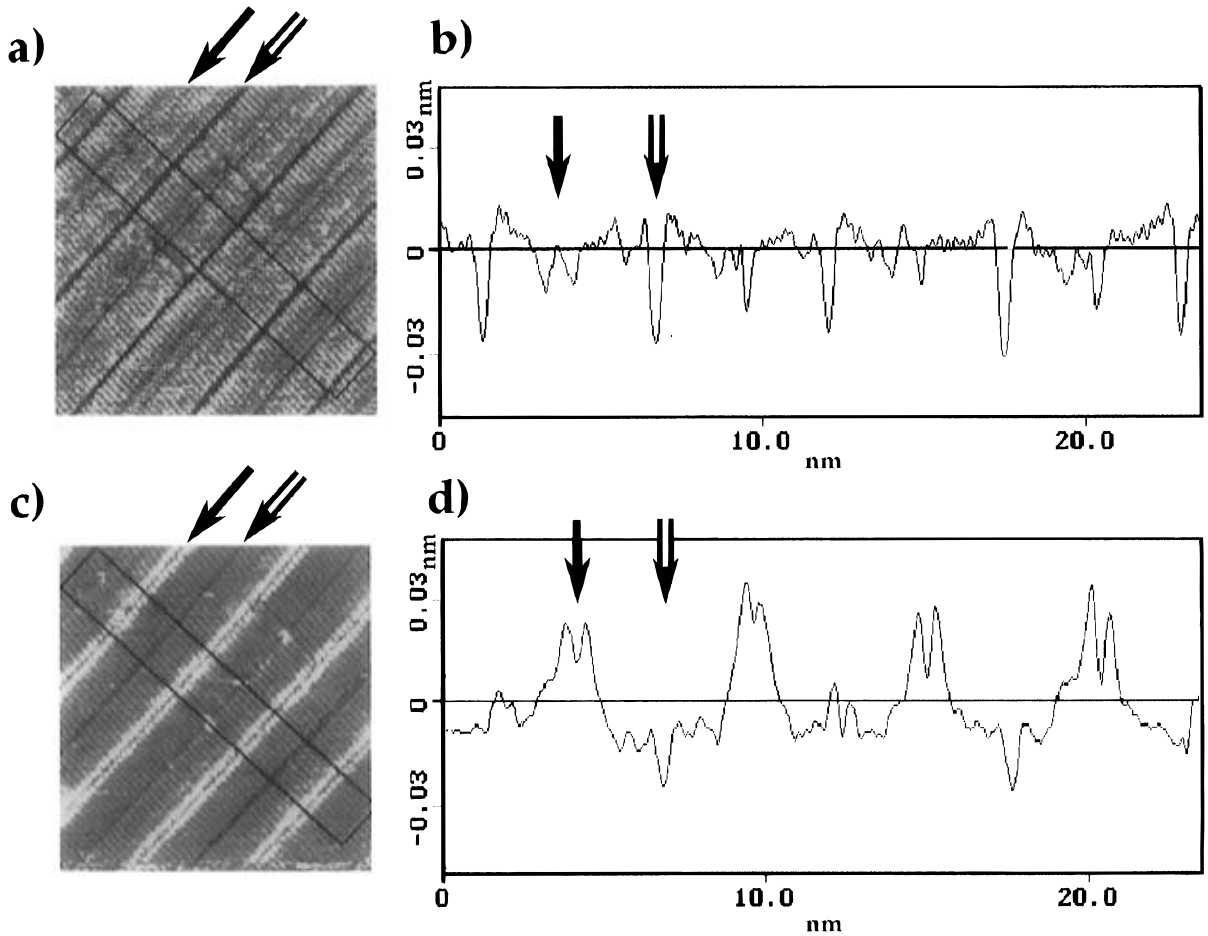

Figure 11. (a) Reproduction of Figure 6a. The area used for the determination of the average cross-section profile in Figure 11b is shown as a black rectangle. (b) Average cross-sectional profile taken perpendicular to the molecular rows (parallel to the molecular axis). The troughs between the rows of bromide molecules are easily differentiated by their relative "depth". The shallow and deep troughs are indicated by → and ⇒, respectively. These labels are used consistently in Figures 6, 7, and 11 for ease of comparison. (c) Reproduction of Figure 7a. The area used for determination of the average cross-sectional profile in Figure 11d, in a region of the film similar to that used in Figure 11a, is shown as a black rectangle. (d) Average cross-sectional profile taken perpendicular to molecular rows (parallel to the molecular axis). The shallow troughs (→) of Figure 11b now appear as two bright spots (→), while the deep troughs (⇒) of Figure 11b remain as deep troughs (⇒). The *Z*-axis of the STM's piezo is *not* calibrated, and the absolute height measurements in this profile are not reliable. However, the relative height of the alkyl chains in the bright and dark bromide images (Figures 6 and 7) are consistent from image to image (compare parts b and d).

on graphite,[7] for example, a dynamic model involving a slip and a twist (a translation and a rotation) of the molecules in the film between two conformers of 2-hexadecylanthraquinone was proposed to interpret the steady-state STM image.

Dramatic variations in the observed contrast associated with the bromine end group in the $CH_3(CH_2)_{21}Br$ film (Figures 6a and 7a) are similar to contrast changes reported for chemisorbed adsorbates. Sautet et al.[36,74,75] observed changes in the image contrast of S atoms chemisorbed on Re(0001), manifested as large changes in the image corrugation just after pulsing the tip voltage or spontaneously during a scan. These changes were attributed to the structural rearrangement of the tip. Calculations of the tunnel current for several tip structures have demonstrated that restructuring of the tip apex (from a single Pt atom to a triangle of 3 Pt atoms) or changes in the tip atom identity (from Pt to S) can have a large impact on the image contrast. The tunneling environment in the liquid droplet when examining physisorbed molecules, such as $CH_3(CH_2)_{21}Br$ on graphite, is even more complex than that for the ultrahigh-vacuum studies of S on Re. It is plausible that the image contrast of our bromine films may change if the tip adsorbs a molecule or an atom from solution, perhaps resulting in a bromine atom terminated tip. Sautet and co-workers also found that changes in the identity of the tip apex atom are associated with changes in resolution, with smaller atoms such as S (for the case of S atoms adsorbed on the tip) yielding higher resolution images. The resolution along the alkyl chains in both dark and bright bromide films (see Figures 6a and 7a, respectively) is quite similar, as is the relative contrast of the alkyl chains in the cross-sectional profile (Figure 11). Of course, these observations alone do not rule out changes in the tip geometry as the cause of the contrast variation. However, if the tip rearranged to a more stable geometry or composition during the experiment, one might expect that the more energetically favorable tip structure would remain fixed; nevertheless, the contrast variation in the physisorbed bromide film (Figures 6a and 7a) is reversible on the time scale of minutes, and a change in tip structure or chemical identity cannot be completely ruled out as a source of this effect.

Clearly the interpretation of the contrast variation in these physisorbed bromide films is complicated by the possibility of molecular motion in the tunnel junction. Molecular motions such as conformational isomerization within the film, if involved in the image contrast change, should be sensitive to temperature variations. We are planning temperature dependent studies in the future to distinguish the effects of variations in the tip from changes in film structure. Additionally, deliberately functionalizing the tip prior to imaging may help stabilize its structure and provide interesting results on the influence of the tip terminal atom on the image contrast.

The possibility that the bromide contrast variation from dark

to bright may be due to molecular reorientation within the film emphasizes the importance of an adsorbate's physical size and spatial orientation during imaging. The alcohol groups, for example, seem to have a contrast similar to that of CH_3 in the STM image (Figure 2a) even though −OH has a larger polarizability than the remainder of the alkyl chain (Figure 9). The orientation of the OH groups in the alcohol film is optimized for hydrogen bonding in the plane of the film (Figure 2b,c), and the frontier orbitals for OH-functionalized hydrocarbons are restricted to lie in the plane of the film. In this orientation the LUMO wave function, localized on the OH group, will not be available for more than average participation in the tunneling process due to poor overlap with the STM tip during imaging. By contrast, the amines appear bright in the STM image (Figure 4a). Examination of a computer model of the amine film (Figure 4b,c) indicates that the lone pair electrons of the NH_2 groups are pointing up out of the film. It should be noted that the spatial distribution of the amine LUMO, localized on the NH_2 group, is quite similar to the location of the N lone pair of the HOMO.[76] This means that the amine LUMO, localized on the NH_2 group, also points up out of the film toward the probing STM tip and is potentially available to participate in the tunneling process since it is spatially extended away from the surface. The orientation of the SH LUMO in the thiol film, unlike the alcohols, is not restricted by a hydrogen-bonding network to lie in the plane of the film, and they appear bright. The orientation of the molecules with respect to the surface, as dictated by intermolecular and molecule−surface interactions within the film (i.e. hydrogen-bonding and van der Waals forces), may control the effective spatial interaction between the tip/surface−adsorbate and be a factor governing the relative image contrast of the functional groups studied here.

Summary

Several functional groups, NH_2, Br, I, and S, have been identified by their bright contrast in STM images of long chain hydrocarbon films physisorbed on graphite. Comparison of the relative brightness of the functional groups confirms an empirical relationship between increasing molecular polarizability and increasing STM image brightness. A model has been proposed in which the molecular adsorbates contribute to the local density of states at the Fermi level of the surface, as monitored by the STM, through an energetically diffuse tail of the adsorbate LUMO, similar to the case of Xe on Ni.[41] Since the adsorbate-induced increase in the LDOS depends only weakly on the difference in energy between the surface Fermi level and the adsorbate LUMO, variations in the tunneling probability, and hence the STM contrast, become more sensitive to the effective spatial overlap between the adsorbate and STM tip than to the details of the adsorbate electronic energies for the group of molecules surveyed here. The extent that the functional groups protrude away from the surface will then determine the degree of tip/surface−adsorbate spatial overlap and will be highly dependent on the adsorbate's physical size (or polarizability), the orientation of the adsorbate with respect to the surface, and the spatial characteristics of the adsorbate LUMO. The electronic structure of the adsorbate is expected to play a larger role in the STM image contrast in cases where the adsorbate LUMO and Fermi level are close in energy, as is the case in conductive organic films.

Acknowledgment. Work at Columbia was supported by the Joint Services Electronics Program (U.S. Army, Navy, and Air Force; DAAHO4-94-G0057), by the Donors of the Petroleum Research Fund administered by the American Chemical Society, by the National Institute of Health, (PHS Grant 1 R03 RR06987-01A1), and by the American Association of University Women. Equipment support was provided by the National Science Foundation (CHE-94-19465). Work at Harvard was supported in part by ARPA and by the Office of Naval Research. We would like to thank Professor Clark Still for an introduction to Macromodel, the program used to generate the computer models presented in this paper, and for a number of stimulating discussions. We are indebted to Dr. Norton Lang for pointing out the importance of the variation in tunnel barrier width in determining the influence of different electronic levels on the tunneling process.

References and Notes

(1) Rabe, J. P.; Buchholz, S.; Askadskaya, L. *Synth. Met.* **1993**, *54*, 339.
(2) Venkataraman, B.; Flynn, G. W.; Wilbur, J.; Folkers, J. P.; Whitesides, G. M. *J. Phys. Chem.* **1995**, *99*, 8684.
(3) Stevens, F.; Walba, D. M. Preprint **1995**.
(4) Spong, J. K.; Mizes, H. A.; LaComb, L. J., Jr.; Dovek, M. M.; Frommer, J. E.; Foster, J. S. *Nature* **1989**, *338*, 137.
(5) Nejoh, H. *Appl. Phys. Lett.* **1990**, *57*, 2907.
(6) Breen, J. J.; Flynn, G. W. *J. Phys. Chem.* **1992**, *96*, 6825.
(7) Stabel, A.; Heinz, R.; Rabe, J. P.; Wegner, G.; Schryver, F. C. D.; Corens, D.; Dehaen, W.; Süling, C. *J. Phys. Chem.* **1995**, *99*, 8690.
(8) Patrick, D. L.; Beebe, T. P. *Langmuir* **1994**, *10*, 298.
(9) Smith, D. P. E. *J. Vac. Sci. Technol. B* **1991**, *9*, 1119.
(10) Venkataraman, B.; Breen, J. J.; Flynn, G. W. *J. Phys. Chem.* **1995**, *99*, 6608.
(11) Wawkuschewski, A.; Cantow, H.-J.; Magonov, S. N. *Langmuir* **1993**, *9*, 2778.
(12) Rabe, J. P.; Buchholz, S. *Science* **1991**, *253*, 424.
(13) Bucher, J.-P.; Roeder, H.; Kern, K. *Surf. Sci.* **1993**, *289*, 370.
(14) Salmeron, M.; Beebe, T.; Odriozola, J.; Wilson, T.; Ogletree, D. R.; Siekhaus, W. *J. Vac. Sci. Technol. A* **1990**, *8* (1), 635.
(15) Liang, W.; Whangbo, M.-H.; Wawkuschewski, A.; Cantow, H. J.; Magonov, S. N. *Adv. Mater.* **1993**, *5*, 817.
(16) Yeo, Y. H.; Yackowboski, K.; McGonigal, G. C.; Thomson, D. J. *J. Vac. Sci. Technol. A* **1992**, *10*, 600.
(17) Biscarini, F.; Bustamante, C.; Kenkre, V. M. *Phys. Rev. B* **1995**, *51*, 11089.
(18) Mizutani, W.; Shigeno, M.; Ono, M.; Kajimura, K. *Appl. Phys. Lett.* **1990**, *56*, 1974.
(19) Mintmire, J. W.; Harrison, J. A.; Colton, R. J.; White, C. T. *J. Vac. Sci. Technol. A* **1992**, *10*, 603.
(20) Ou-Yang, H.; Marcus, R. A.; Källebring, B. *J. Chem. Phys.* **1994**, *100*, 7814.
(21) Winkler, R. G.; Hentschke, R. *J. Chem. Phys.* **1994**, *100*, 3930.
(22) Thibaudau, R.; Watel, G.; Cousty, J. *Surf. Sci. Lett.* **1993**, *281*, L303.
(23) Wawkuschewski, A.; Cantow, H.-J.; Magonov, S. N.; Möller, M.; Liang, W.; Whangbo, M.-H. *Adv. Mater.* **1993**, *5*, 821.
(24) Hara, M.; Iwakabe, Y.; Tochigi, K.; Sasabe, H.; Garito, A. F.; Yamada, A. *Nature* **1990**, *344*, 228.
(25) Morozov, V. N.; Seeman, N. C.; Kallenbach, N. R. *Scanning Microsc.* **1993**, *7*, 757.
(26) Fisher, A. J.; Blöchl, P. E. *Phys. Rev. Lett.* **1993**, *70*, 3263.
(27) Poler, J. C.; Zimmerman, R. M.; Cox, E. C. *Langmuir* **1995**, *11*, 2689.
(28) Sleator, T.; Tycko, R. *Phys. Rev. Lett.* **1988**, *60*, 1418.
(29) Lupkowski, M.; Maguire, J. F. *Compos. Interfaces* **1994**, *2*, 1.
(30) McGonigal, G. C.; Bernhadt, R. H.; Thomson, D. J. *Appl. Phys. Lett.* **1990**, *57*, 28.
(31) Yackoboski, K.; Yeo, Y. H.; McGonigal, G. C.; Thomson, D. J. *Ultramicroscopy* **1992**, *42*−*44*, 963.
(32) Lindsay, S. M.; Sankey, O. F.; Li, Y.; C., H.; Rupprecht, A. *J. Phys. Chem.* **1990**, *94*, 4655.
(33) Smith, D. P. E.; Hörber, J. K. H.; Binning, G.; Nejoh, H. *Nature* **1990**, *344*, 641.
(34) Walba, D. M.; Stevens, F.; Parks, D.; Clark, N.; Wand, M. *Science* **1995**, *267*, 1144.
(35) Hallmark, V. M.; Chiang, S.; Meinhardt, K.-P.; Hafner, K. *Phys. Rev. Lett.* **1993**, *70*, 3740.
(36) Sautet, P.; Joachim, C. *Chem. Phys. Lett.* **1991**, *185*, 23.
(37) Ludwig, Z. *Phys. B* **1992**, *86*, 397.
(38) Ludwig, Z. *Phys. B* **1994**, *93*, 375.
(39) Traven, V. F. *Frontier Orbitals and Properties of Organic Molecules*; Ellis Horwood: New York, 1992.
(40) Ukraintsev, V. A.; Long, T. J.; Gowl, T.; Harrison, I. *J. Chem. Phys.* **1992**, *96*, 9114.

(41) Eigler, D. M.; Weiss, P. S.; Schweizer, E. K.; Lang, N. D. *Phys. Rev. Lett.* **1991**, *66*, 1189.
(42) Somorjai, G. A. *Introduction to Surface Chemistry and Catalysis*; Wiley-Interscience: New York, 1994.
(43) Weber, R. R.; Peria, W. T. *Surf. Sci.* **1969**, *14*, 13.
(44) Antoniewicz, P. R. *Surf. Sci.* **1975**, *52*, 703.
(45) The Whitesides group at Harvard have synthesized and purified the $CH_3(CH_2)_{21}SH$ samples as previously described in the following: Bain, C. D.; Troughton, E. B.; Tao, Y.-T.; Evall, J.; Whitesides, G. M.; Nuzzo, R. G. *J. Am. Chem. Soc.* **1989**, *111*, 321.
(46) Macromodel is a program developed by Prof. Clark Still's group at Columbia University.
(47) Weiner, S. J.; Kollman, P. A.; Case, D. A.; Singh, U. C.; Ghio, C.; Alagona, G.; Profeta, S., Jr.; Weiner, P. *J. Am. Chem. Soc.* **1984**, *106*, 765.
(48) Findenegg, G. H. *J. Chem. Soc., Faraday Trans.* **1972**, *68*, 1799.
(49) Groszek, A. J. *J. Proc. R. Soc. London* **1970**, *314*, 473.
(50) Leggetter, S.; Tildesley, D. J. *Ber. Bunsen-Ges. Phys. Chem.* **1990**, *94*, 285.
(51) Elbel, N.; Günther, E.; Seggern, H. *Appl. Phys. Lett.* **1994**, *65*, 642.
(52) Cyr, D. M.; Flynn, G. W. Unpublished Results. Sulfurs appear bright for both $CH_3(CH_2)_{21}SS(CH_2)_{21}CH_3$ and $CH_3(CH_2)_{17}S(CH_2)_{17}CH_3$ on both graphite and MoS_2 surfaces.
(53) Liu, X.; Zheng, J. F.; Weber, E. R.; Salmeron, M.
(54) Hoshino, A.; Isoda, S.; Kurata, H.; Kobayashi, T. *J. Cryst. Growth* **1995**, *146*, 636.
(55) *Handbook of Chemistry and Physics*, 71st ed.; CRC Press, Inc.: Boston, 1990−91.
(56) Tersoff, J.; Hamman, D. R. *Phys. Rev. Lett.* **1983**, *50*, 1998.
(57) Tersoff, J.; Hamann, D. R. *Phys. Rev. B* **1985**, *31*, 805.
(58) Sautet, P.; Bocquet, M.-L. *Surf. Sci. Lett.* **1994**, *304*, 445.
(59) Magonov, S. N.; Wawkuschewski, A.; Cantow, H.-J.; Liang, W.; Whangbo, M.-H. *Appl. Phys.* **1994**, *59*, 119.
(60) Cyr, D. M.; Flynn, G. W. Unpublished results.
(61) Hibino, M.; Sumi, A.; Hatta, I. *Jpn. J. Appl. Phys.* **1995**, *34*, 3354.
(62) Jung, T.; Mo, Y. W.; Himpsel, F. J. *Phys. Rev. Lett.* **1995**, *74*, 1641.
(63) Maroncelli, M.; Strauss, H. L.; Snyder, R. G. *J. Chem. Phys.* **1985**, *82*, 2811.
(64) Synder, R. G.; Maroncelli, M.; Qi, S. P.; Strauss, H. L. *Science* **1981**, *214*, 188.
(65) Lévay, B.; Lalovic, M.; Ache, H. J. *J. Chem. Phys.* **1989**, *90*, 3282.
(66) Hoffman, J. D. *J. Chem. Phys.* **1952**, *20*, 541.
(67) Sirota, E. B.; King, J. H. E.; Singer, D. M.; Shao, H. H. *J. Chem. Phys.* **1993**, *98*, 5809.
(68) Ungar, G. *J. Phys. Chem.* **1983**, *87*, 689.
(69) McClure, D. W. *J. Chem. Phys.* **1968**, *49*, 1830.
(70) Momany, F. A.; Bonham, R. A.; McCoy, W. H. *J. Am. Chem. Soc.* **1963**, *85*, 3077.
(71) Komaki, C.; Ichishima, I.; Kuratani, K.; Miyazawa, T.; Shimanouchi, T.; Mizushima, S.-I. **1955**, *28*, 330.
(72) Askadskaya, L.; Rabe, J. P. *Phys. Rev. Lett.* **1992**, *69*, 1395.
(73) Reinhard, H.; Schürmann, B. L.; Rabe, J. P. *J. Chem. Phys.* **1992**, *96*, 6213.
(74) Sautet, P.; Dunphy, J. C.; Ogletree, D. F.; Joachim, C.; Salmeron, M. *Surf. Sci.* **1994**, *315*.
(75) McIntyre, B. J.; Sautet, P.; Dunphy, J. C.; Salmeron, M.; Somorjai, G. A. *J. Vac. Sci. Technol. B* **1994**, *12*, 1751.
(76) Jorgensen, W. L.; Salem, L. *The Organic Chemist's Book of Orbitals*; Academic Press: New York, 1973.

JP9606467